Understanding the submicron domain structure of MnAs thin films on GaAs(001): Magnetic force microscopy measurements and simulations

R. Engel-Herbert, J. Mohanty, A. Ney, T. Hesjedal,[a] L. Däweritz, and K. H. Ploog
Paul-Drude-Institut für Festkörperelektronik, Hausvogteiplatz 5–7, D-10117 Berlin, Germany

(Received 24 September 2003; accepted 4 December 2003)

Over a wide temperature range of 30 °C around room temperature, MnAs films on GaAs(001) semiconductor substrates break up into ordered arrays of submicron-sized ferromagnetic α and paramagnetic β wires. Both the hard and the easy axis of magnetization (perpendicular to the wires) lie in the film plane and a large variety of complex domain patterns are found in micromagnetic investigations with magnetic force microscopy (MFM). A systematic analysis of the domain configurations is given and the most likely configurations are identified through MFM contrast simulations. © *2004 American Institute of Physics.* [DOI: 10.1063/1.1645328]

The combination of ferromagnetic and semiconducting materials is the prerequisite for devices that make use not only of the charge of the electron but also of its spin.[1] Ferromagnetic MnAs on GaAs is a promising candidate for future spintronic devices.[2] Epitaxial MnAs$(1\bar{1}00)$ films of high quality can be grown by molecular beam epitaxy (MBE) on, e.g., GaAs(001).[3–6] Bulk MnAs shows a first order phase transition from the ferromagnetic, hexagonal α phase to the paramagnetic, orthorhombic β phase at about 40 °C.[7] In epitaxial MnAs films the phase transition is more complex and leads, due to the involved composition-dependent strain, to a wide coexistence region of both phases of 10–40 °C.[6] In this temperature region, a self-organized array of α- and β-MnAs wires is found where the width of the α wires is a function of temperature.[8,9] The array can be easily observed, see Fig. 1(b), as the thickness of the α wires is about 1.2% larger than that of the β wires. The surface modulation due to the phase coexistence was described within an elastic model and results in almost rectangular cross sections of the wires.[8] In this letter, we present a systematic analysis of the domain configurations in this magnetic wire system and identify the micromagnetic structure through magnetic force microscopy (MFM) contrast simulations.

The epitaxial MnAs samples were grown on GaAs(001) wafers at 250 °C by standard solid-source MBE.[5] Under As-rich growth conditions, the so-called A orientation is predominantly obtained with MnAs$(1\bar{1}00)\|$GaAs(001) and MnAs$[0001]$ (c axis)$\|$GaAs$[1\bar{1}0]$.[5] The investigated films have various thicknesses around 200 nm.

The magnetic properties of the films were determined using a superconducting quantum interference device (SQUID) magnetometer. MnAs exhibits a strong uniaxial in-plane anisotropy with MnAs$[11\bar{2}0]$ being the easy axis of magnetization (a axis) and MnAs$[0001]$ the hard axis of magnetization (c axis).[6] This is a rather uncommon situation, as the out-of-plane anisotropy field ($\sim$1.0 T) is smaller than the in-plane one ($\sim$2.0 T).[6] The ferromagnetic α phase has the hexagonal NiAs ($B8_1$) structure with an ABACABAC… stacking and Mn atoms on A and As atoms on B and C sites, respectively. The direct exchange coupling is unlikely between Mn atoms along the a axis due to the large distance. Hence, in MnAs, ferromagnetism is due to the indirect exchange between Mn atoms via As atoms.[10]

The micromagnetic investigations were performed using a MFM that was equipped with a variable temperature stage in order to control the width of the ferromagnetic wires and thus select specific domain configurations. MFM is based on noncontact force microscopy and employs ferromagnetically coated tips that are magnetized along the tip axis with a permanent magnet (800 Oe). This makes the MFM predominantly sensitive towards out-of-plane components of the sample's stray field. The measured signal is proportional to the second derivative of the stray field.[11] Depending on the tip-sample distance, it is possible to be primarily sensitive to the surface topography through the short range van der Waal's force, or, to the longer range magnetic interaction. The particular interaction between the tip's and the sample's stray field depends on the tip shape, its thickness and choice of magnetic material, as well as on the scan height above the sample. Eighty nanometer Cr–Co coated Si cantilevers were used for the experiments.[12]

Figure 1 shows a representative MFM scan (a) of a demagnetized 180-nm-thick MnAs film at zero magnetic field and at room temperature and the corresponding topography (b). The ferromagnetic α and paramagnetic β wires, as well

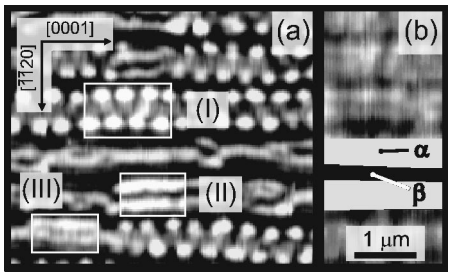

FIG. 1. Typical domain patterns of a 180-nm-thick MnAs film at 21 °C; (a) magnetic contrast at zero magnetic field, (b) topography for illustrating the geometrical boundary of the ferromagnetic wires (bright). Characteristic domain configurations, classified by the number of subdivisions along the MnAs$[11\bar{2}0]$ direction, are highlighted. The type (I), (II), and (III) configurations denote one, two, and three subdivisions, respectively.

[a]Author to whom correspondence should be addressed; electronic mail: hesjedal@pdi-berlin.de

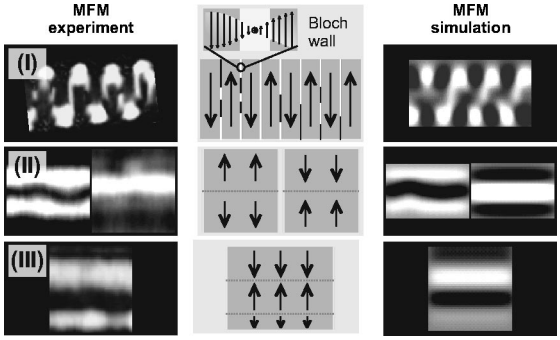

FIG. 2. Comparison of the measured domain patterns (left column), the most probable domain configurations (middle column), and the simulated MFM contrast (right column) for the common domain types (I-III). Black and white lines in the domain configuration pictures indicate 180° Bloch domain walls pointing out of and into the surface plane, respectively. The dotted gray lines mark the border between subdomains.

as the crystal orientation, are indicated in the figure. Domains are formed in ferromagnetic materials in order to minimize the magnetic stray field energy. The domain structure is thus a consequence of the limited dimensions of the ferromagnet. SQUID measurements were carried out in and out of plane (not shown), revealing that virtually all moments lie in the film plane along the MnAs$[\bar{1}120]$ direction. Consequently, the MFM contrast is due to the stray field of the individual bar magnets and the 180° Bloch walls that separate domains of opposite orientation. In the investigated temperature range (below 40 °C), out-of-plane magnetized ferromagnetic clusters have no apparent influence on the contrast.[13]

Three typical domain configurations are highlighted in Fig. 1, marked (I), (II), and (III). The classification is based on the number of subdivisions along the easy-axis direction. The simplest configuration, type (I), consists of one subdivision, i.e., the whole wire is either magnetized parallel or antiparallel to the $[\bar{1}120]$ direction across its width. In the demagnetized state, the individual bar magnets line up with alternating orientation along the wire (in the [0001] direction), separated by 180° Bloch walls, leading to a zig-zag-shaped contrast in MFM. Alternating type (I) domains are present in the temperature range from around 10 to 30 °C and have a temperature-independent average width in the [0001] direction of 190 nm. Below 10 °C, the MnAs wires have expanded in width to a degree where the magnetic behavior is governed by the inter-wire coupling, favoring domains that stretch across several wires.[14] Above the upper temperature limit, the wires narrow below a critical limit where only one subdivision is stable. However, only type (I) domains that are extended in the [0001] direction are then observed. It should be noted that the transformation of the extended domains upon cooling does not necessarily proceed via the type (I) domains into the coupled wire phase below 10 °C. The type (II) domains have two possible configurations of the two subdomains, as illustrated in Fig. 2(II), with the moments facing each other or pointing away from each other. Triple-split domains [type (III)] have a more complex appearance. They exist in an unevenly split subdomain partitioning [see Fig. 2(III)] with the respective configurations. From MFM temperature cycles it is known that the third subdomain appears upon cooling gradually, leading to an even partitioning ratio at room temperature. If the wire is more strongly strained, e.g., near a wire junction or termination, the wire expansion occurs suddenly and evenly partitioned subdomains appear even at higher temperatures.

In order to understand the domain structure that leads to the apparent MFM image, we performed simulations of the MFM contrast.[11] The simulation consists of an analysis of the MFM response, followed by calculating the stray field of the assumed micromagnetic structure of the sample and the magnetized tip. An alternative formulation of the problem is given by Ref. 15. The total force acting on the tip due to the magnetic stray field of the sample is given by: $\mathbf{F}_{\mathrm{tot}}(\mathbf{r}) = \int_{\mathrm{tip}}(\mathbf{M}_{\mathrm{tip}}(\mathbf{r}')\cdot\nabla_{\mathbf{r}})\mathbf{B}_{\mathrm{sample}}(\mathbf{r}-\mathbf{r}')d^3\mathbf{r}'$, i.e., the force is obtained by assuming the tip to be composed of dipoles interacting with the external magnetic field of the sample. As the MFM is based on noncontact mode force microscopy, the measured quantity is the frequency shift which is proportional to the derivative of the normal component of the total tip-sample interaction force (normal means perpendicular to the cantilever surface).

For simplification it is assumed that the magnetizations of tip $[\mathbf{M}_{\mathrm{tip}}=(0,0,M_z)]$ and sample are absolutely hard and therefore not able to influence each other. Furthermore, the unit vector along z is collinear to the surface normal of the sample: $\mathbf{n}=\mathbf{e}_z$. Now, only the z component of the total force gradient contributes to the frequency shift, yielding:

$$F_z'(\mathbf{r}) = \int_{\mathrm{tip}} \left(M_z(\mathbf{r}')\cdot\frac{\partial^2}{\partial z^2}B_z(\mathbf{r}-\mathbf{r}')d^3\mathbf{r}' \right). \tag{1}$$

For the calculations the tip is assumed to be a spherically shaped surface with a radius of 120 nm.

We simulate the interaction between the tip and the stray field of the sample, originating from a given distribution of magnetic moments. Reasonable magnetization distributions are assumed, based on the information from SQUID measurements. The stray field is derived with the help of the magnetostatic potential, taking only magnetic dipoles into account and by integrating the elementary dipoles over the sample volume. It is further assumed that the magnetic dipole strength is constant and uniformly distributed. The direction of the magnetic dipoles is variable, because the total stray field consists of two different contributions: domains with an in-plane magnetization along the easy axis and the Bloch walls exhibiting an out-of-plane magnetization. This results in different distance dependencies of the in-plane and out-of-plane magnetic stray field components in the z direction. The thickness of the Bloch wall was estimated from MFM measurements to be roughly 10 nm, as the exchange stiffness A of MnAs is presently not known.

Figure 2 shows the comparison of the measured MFM contrast and the simulated contrast for the proposed domain configurations for types (I-III). Type (I) domains, where the wires are single domain across its width, are typical for the upper and lower limit of the temperature coexistence region of α and β MnAs. Very narrow wires tend to be also single domain along their whole length (in [0001] direction) of some μm. The alternating type (I) domains are appearing as zig-zag shaped at lower resolution (i.e., higher working distance). At higher resolution, bright areas are visible at the

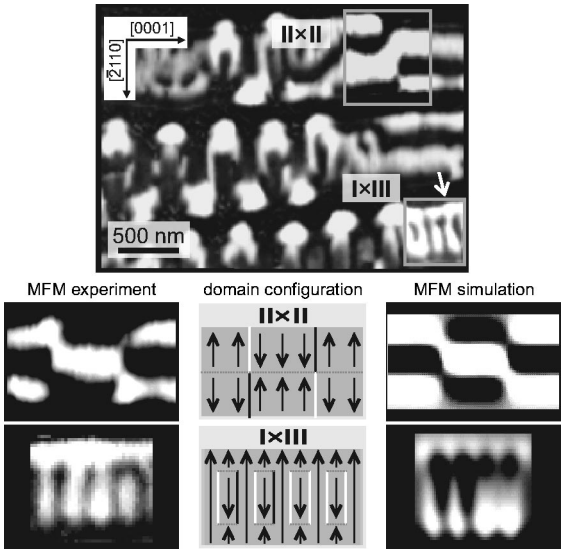

FIG. 3. MFM overview scan of a sample area with more complex domain boundaries (above). The highlighted areas denote boundaries between two type (II), (II×II) and type (I) and (III) domains, (I×III), respectively. The comparison between experiment and simulation for the assumed domain configuration is shown below.

ends of the antiparallely magnetized bar magnets. In between the domains, the contrast is due to differently oriented Bloch walls, either rotating the moments through the direction pointing out of or into the surface plane, respectively. This contrast is modeled correctly, as shown on the right-hand side of Fig. 2(I), assuming the sketched distribution of magnetic moments. The type (II) domains exist in two variations [cf. Fig. 2(II)] with the in-plane moments pointing towards or away from each other. Interestingly, the addition of a third subdomain during the expansion of the ferromagnetic wire (upon cooling) occurs gradually and not necessarily abruptly by rearrangement of the magnetic subdivisions. Therefore, it is reasonable that the proposed domain configuration for the type (III) domains [cf. Fig. 2 (bottom)], has an uneven ratio of the subdomains. It has to be noted that for domain types (II) and (III), neither a Bloch nor a Néel domain wall along the length of the wire was included in the simulations. The possible absence of a domain wall is presumably due to the fact that there is no direct exchange coupling between neighboring Mn atoms along the *a* axis.[10]

Next, we took a closer look at more complex domain boundaries, that is, between two type (II), (II×II), and between type (I) and (III) domains, (I×III). In Fig. 3, the MFM overview scan shows some of the most prominent boundaries. First, the domain boundaries between type (I) domains of antiparallel alignment of the magnetic moments are well resolved in this image. With less lateral resolution, these domains appear as zig-zag shaped, as explained above. The domain boundaries of type (II×II) and (I×III) are highlighted and marked in the image. Below, two prominent domain boundaries of this type are shown in experiment and simulation. A domain boundary between two evenly divided type (II) domains is quite simple, as only two configurations exist [cf. Fig. 2(II)]. The asymmetry in the MFM picture is, however, not due to the tip shape, but due to Bloch walls between the two subdomains as indicated by black and white lines in the domain configuration images of Fig. 3. The orientation of the Bloch wall was obtained by finding the best agreement with the simulated image. Similarly, the Bloch wall orientation is also responsible for the tilted appearance of the domain pattern in the case of the (I×III) domain boundary (see arrow in Fig. 3, above), contrary to the appearance in Fig. 1. Again, the simulation allows for the extraction of the Bloch wall orientation. Basically, the (I×III) domain boundary is due to a sequence of type (I) and (III) domains with variable width and length of the subdivisions. The width and length of the individual domains were used as a fitting parameter for the simulation. We are well aware that this magnetic system is quite complex and that the present model is rather limited. However, it allows for the extraction of the most likely domain configurations as a good agreement between the modeled and measured MFM contrast is obtained.

In summary, we have presented a systematic investigation of the domain patterns of ferromagnetic MnAs wires on GaAs(001) by atomic force microscopy, MFM and SQUID magnetometry. The submicron wire size can be tuned via the temperature, giving rise to a large variety of domain configurations. MnAs exhibits a strong uniaxial in-plane anisotropy with the easy (*a* axis) and hard axis (*c* axis) of magnetization being in plane and perpendicular to each other. Three classes of domains can be distinguished by the number of subdomains along the easy-axis direction. Between the subdomains, i.e., within a domain class, the MFM contrast suggests the absence of a Bloch wall. Complex domain boundaries between different domain classes, involving Bloch walls, can be understood via modeling of the MFM contrast.

The authors would like to thank C. Herrmann and M. Kästner for sample growth. Part of this work was sponsored by the BMBF, Germany.

[1] G. A. Prinz, Science **250**, 1092 (1990).
[2] M. Ramsteiner, H. Y. Hao, A. Kawaharazuka, H. J. Zhu, M. Kästner, R. Hey, L. Däweritz, H. T. Grahn, and K. H. Ploog, Phys. Rev. B **66**, 081304(R) (2002).
[3] M. Tanaka, J. P. Harbison, M. C. Park, Y. S. Park, T. Shin, and G. M. Rothberg, J. Appl. Phys. **76**, 6278 (1994).
[4] M. Tanaka, Physica E (Amsterdam) **2**, 372 (1998).
[5] F. Schippan, A. Trampert, L. Däweritz, and K. H. Ploog, J. Vac. Sci. Technol. B **17**, 1716 (1999).
[6] F. Schippan, G. Behme, L. Däweritz, K. H. Ploog, B. Dennis, K.-U. Neumann, and K. R. A. Ziebeck, J. Appl. Phys. **88**, 2766 (2000).
[7] C. Guillaud, J. Phys. Radium **12**, 223 (1954).
[8] T. Plake, M. Ramsteiner, V. M. Kaganer, B. Jenichen, M. Kästner, L. Däweritz, and K. H. Ploog, Appl. Phys. Lett. **80**, 2523 (2002).
[9] T. Plake, T. Hesjedal, J. Mohanty, M. Kästner, L. Däweritz, and K. H. Ploog, Appl. Phys. Lett. **82**, 2308 (2003).
[10] A. K. Das, C. Pampuch, A. Ney, T. Hesjedal, L. Däweritz, R. Koch, and K. H. Ploog, Phys. Rev. Lett. **91**, 087203 (2003).
[11] D. Sarid, *Scanning Force Microscopy: With Applications to Electric, Magnetic and Atomic Forces* (Oxford University Press, Oxford, 1994); A. Hubert and R. Schäfer, *Magnetic Domains* (Springer, Berlin, 1998).
[12] MikroMasch MSC12, Tallinn, Estonia.
[13] A. Ney, T. Hesjedal, C. Pampuch, J. Mohanty, A. K. Das, L. Däweritz, R. Koch, and K. H. Ploog, Appl. Phys. Lett. **83**, 2850 (2003).
[14] E. Bauer, S. Cherifi, L. Daeweritz, M. Kaestner, S. Heun, and A. Locatelli, J. Vac. Sci. Technol. B **20**, 2539 (2002).
[15] A. Hubert, W. Rave, and S. L. Tomlinson, Phys. Status Solidi B **204**, 817 (1997).